Energy Advances

ROYAL SOCIETY OF CHEMISTRY

PAPER

View Article Online
View Journal | View Issue

Cite this: *Energy Adv.*, 2024, 3, 997

Bamboo charcoal as electrode material for vanadium redox flow batteries†

Monja Schilling,[a] Alexey Ershov,[b] Rafaela Debastiani,[cd] Kangjun Duan,[a] Kerstin Köble,[a] Simon Scherer,[a] Linghan Lan,[e] Alexander Rampf,[a] Tomáš Faragó,[b] Marcus Zuber,[f] Angelica Cecilia,[b] Shaojun Liu,[ag] Cheng Liu,[ag] Tilo Baumbach,[bf] Jun Li,[e] Pang-Chieh Sui[gh] and Roswitha Zeis *[aij]

Large-scale energy storage is becoming more critical since the share of energy from renewable sources has increased steadily in recent years. Vanadium redox flow batteries (VRFBs) are a promising candidate for such applications. However, this technique still needs to overcome challenges to enhance battery efficiency, and the investigation of new electrode materials is crucial in this process. In this study, we evaluate bamboo charcoal (BC) as an electrode material for VRFBs for the first time. Bamboo is a rapidly growing renewable carbon source and is thermally treated for use in electrochemical applications. The structure, wettability, wetting behavior, and electrochemical performance of differently-doped BC electrodes are investigated in detail. Scanning electron microscopy and X-ray micro- and nano-computed tomography show the promising channel structure of BC, beneficial for the electrolyte transport through the electrode. Additionally, synchrotron-based time-resolved X-ray radiography and micro tomography was used for an *in situ* study of the electrolyte flow through the BC channels. These investigations and the dynamic vapor sorption measurements prove that the aqueous electrolyte wets the material easily. Furthermore, we studied the electrochemical performance using cyclic voltammetry and electrochemical impedance spectroscopy combined with the distribution of relaxation times analysis. The undoped BC turned out to have a high catalytic activity towards the vanadium redox reaction, whereas the N-doped BC exhibits improved wettability. In conclusion, BC has great potential to be a suitable and renewable VRFB electrode material.

Received 10th March 2024,
Accepted 30th April 2024

DOI: 10.1039/d4ya00166d

rsc.li/energy-advances

Introduction

Large-scale energy devices are needed to store excess energy from renewable sources to balance energy fluctuations and ensure a stable and reliable electrical grid. The Vanadium redox flow battery (VRFB) is a commercially available technology that can help to achieve this goal. VRFBs consist of an electrochemical cell connected to sizeable external electrolyte tanks storing the energy. The electrochemical reactions for charging and discharging the battery occur at the electrochemically active sites of the electrode material in the cell. Carbon-based porous materials such as carbon felt, carbon paper, or carbon cloth are used as electrode materials, often fabricated from raw oil (*e.g.*, PAN-based materials) or cellulose (*e.g.*, Rayon-based materials).[1–3] However, research groups worldwide are exploring different materials as precursors for carbon-based electrodes. Bio-derived materials such as bamboo charcoal are attractive for different energy storage applications such as microbial fuel cells,[4,5] solar thermal energy storage devices,[6,7] and supercapacitors.[8] Additionally, many research groups are inspired by bamboo's natural channel structure and fabricate electrode materials with bamboo-like structures,

[a] *Karlsruhe Institute of Technology, Helmholtz Institute Ulm, Helmholtzstraße 11, D-89081 Ulm, Germany*
[b] *Karlsruhe Institute of Technology, Institute for Photon Science and Synchrotron Radiation, KIT Campus North, Hermann-von-Helmholtz-Platz 1, D-76344 Eggenstein-Leopoldshafen, Germany*
[c] *Institute of Nanotechnology (INT), Karlsruhe Institute of Technology (KIT), Kaiserstraße 12, 76131 Karlsruhe, Germany*
[d] *Karlsruhe Nano Micro Facility (KNMFi), Karlsruhe Institute of Technology (KIT), Hermann-von-Helmholtz-Platz 1, 76344 Eggenstein-Leopoldshafen, Germany*
[e] *Key Laboratory of Low-Grade Energy Utilization Technologies and Systems, School of Energy and Power Engineering, Chongqing University, Chongqing 400030, China*
[f] *Karlsruhe Institute of Technology, Laboratory for Applications of Synchrotron Radiation, KIT Campus South, Kaiserstr. 12, D-76131 Karlsruhe, Germany*
[g] *School of Automotive Engineering, Wuhan University of Technology, Wuhan 430070, China*
[h] *Institute for Integrated Energy Systems, University of Victoria, Victoria, BC V8W 2Y2, Canada*
[i] *Friedrich-Alexander-Universität Erlangen-Nürnberg (FAU), Faculty of Engineering, Department of Electrical, Electronics, and Communication Engineering, Cauerstraße 9, D-91058 Erlangen, Germany. E-mail: roswitha.zeis@fau.de*
[j] *Department of Mechanical & Industrial Engineering, University of Toronto, 5 King's College Road, Toronto, Ontario, M5S 3G8, Canada*

† Electronic supplementary information (ESI) available: Video 1: μ-CT. Video 2: Synchrotron X-ray radiography of the electrolyte injection. See DOI: https://doi.org/10.1039/d4ya00166d

which show promising behavior for the electrochemical performance.[9–13]

Bamboo is a common grass-like plant that rapidly grows in the Asia-Pacific region.[14] This natural functionally hierarchical material consists of parenchyma cells and vascular bundles, part of the plant's water transport system.[15–18] The peculiar structure of bamboo provides an efficient water transport system with high flux, allowing the plant to grow rapidly.[19] This structure was previously studied with, *e.g.*, optical microscopy,[15,18] micro-computed tomography (μ-CT),[17,18] and atomic force microscopy.[15]

For use in energy storage devices, bamboo is carbonized at high temperatures. During this thermal treatment, the characteristic porous structure of the bamboo is preserved, and the obtained Bamboo Charcoal (BC) has a high electrical conductivity.[4,7] Due to bamboo's high abundance and fast growth, BC is a cheap bio-derived material. It can be used as BC tubes[4,5,7] or ground to BC powder[13] to prepare an electrode.

Electrodes for VRFBs must have a structure enabling an easy electrolyte transport to avoid pumping losses and ensure that the active species in the electrolyte reach the reaction sites of the electrode material. The porous, channel-like structure of BC might be potentially suitable for electrolyte transport through the electrode. Nevertheless, to our knowledge, there are no reports about using BC tubes as VRFB electrodes.

Herein, we report on fabricating and testing BC tube-based electrodes for VRFBs. The first part of the work is devoted to the investigation of the material structure on different length scales by using laboratory source based micro- and nano-X-ray computed tomography (μ-CT, nano-CT), and scanning electron microscopy (SEM). The second part describes an *in situ* study of the dynamics of the electrolyte flow in the electrode by employing synchrotron radiography and tomography. Here, the high flux and partial coherence of synchrotron beam allow to visualize the electrolyte permeation and distribution within the electrode BC channels with a high time resolution. Additionally, since the material's surface needs to be sufficiently wetted to utilize the electrochemically active sites, the wettability of the material was investigated *via* dynamic vapor sorption (DVS) measurements. Last, the electrochemical performance of undoped and N-doped BC tubes was characterized using electrochemical impedance spectroscopy (EIS) combined with the distribution of relaxation times (DRT) analysis and cyclic Voltammetry (CV).

Experimental

Materials and electrolyte preparation

Vanadium(IV) electrolyte (0.1 M $VOSO_4$ in 2 M H_2SO_4) was prepared by dissolving $VOSO_4$ (vanadyl sulfate hydrate, 99.9% metal basis, Thermo Fisher Scientific) in diluted H_2SO_4 (diluted from concentrated sulfuric acid, 96%, Suprapur®, Merck with ultrapure water (18.2 MΩ cm)). This electrolyte was used for the

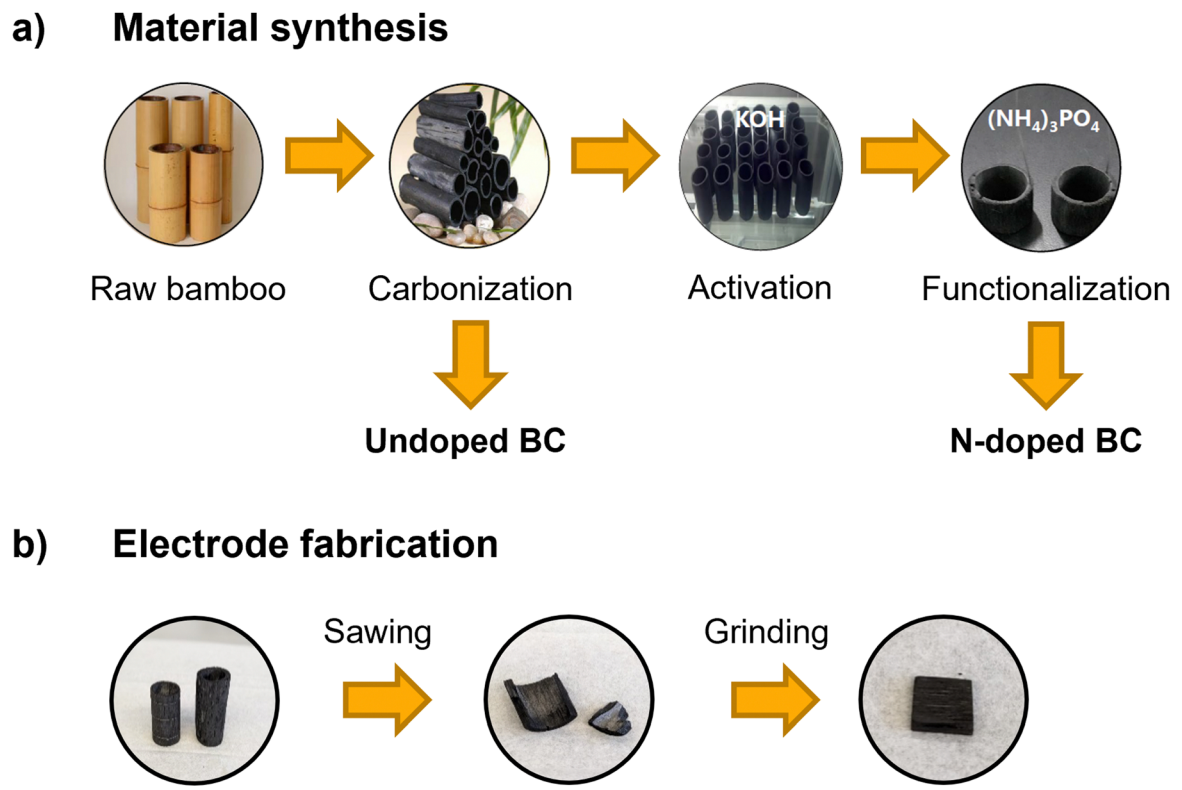

Fig. 1 (a) Preparation process of undoped and N-doped bamboo charcoal (BC) starting from raw bamboo and (b) scheme of electrode fabrication for electrochemical measurements.

electrochemical measurements with the positive half-cell setup and for the synchrotron X-ray imaging experiments.

The bamboo charcoal pieces were prepared from *phyllostachys pubescens*, harvested in the Sichuan province (China). The preparation process from raw bamboo to small pieces of bamboo charcoal is depicted in Fig. 1 and has already been established for BC used in different energy applications.[4,5,7] Bamboo pieces were cut from the plants, washed with deionized water, and dried in an oven (WGL-125B, TAISITE Instrument) at 80 °C. Subsequently, the bamboo pieces were carbonized in a tubular furnace (JQF1100-30, Tianjin Zhonghuan Lab Furnace Co., Ltd) in a nitrogen atmosphere at 1000 °C for 2 h. These BC samples are referred to as undoped BC in the following. An activation step and a functionalization step were performed for the doped sample afterward. During activation, the BC was soaked in a 50 wt% KOH aqueous solution (Guangdong Guanghua Sci-Tech Co., Ltd) for 12 h and thermally treated in a nitrogen atmosphere at 800 °C for 2 h. For the functionalization, these samples were further soaked in saturated $(NH_4)_3PO_4$ (98%, Tianjin Guangfu Fine Chemical Research Institute) solution for 12 h and thermally treated in a nitrogen atmosphere at 900 °C for 2 h. These final BC samples are called N-doped BC.

A detailed analysis including X-ray photoelectron spectroscopy, elemental analysis, and X-ray diffraction spectroscopy of the undoped BC and N-doped BC samples can be found here.[13]

For implementing the BC in the flow cell (detailed description in the next section), small pieces of 1.0 cm × 1.0 cm are required. The BC tubes were cut into pieces with a jigsaw and ground with sandpaper to achieve the desired size.

Imaging methods for analyzing the morphology of BC electrodes and the electrolyte flow

The BC's structure was visualized using SEM, μ-CT, and nano-CT. In detail, the SEM measurements were conducted with a LEO 1550 VP (Carl Zeiss AG, InLens detector, 3 keV acceleration voltage). The μ-CT measurement was performed with an Xradia 510 Versa X-ray microscope (Carl Zeiss AG). A resolution of 1 μm was achieved, and the software *Dragonfly*[20] was used to analyze the data. A median filter was used for the data treatment, and the built-in deep learning tools were employed to quickly and accurately segment the images.

A small sample scraped from an undoped BC tube was glued on a needle and scanned using the lab-based nano-CT Xradia 810 Ultra (Carl Zeiss AG).[21] This system operates with a quasi-monochromatic X-ray beam from a Cr anode (energy of 5.4 keV) and a sequence of optics to obtain a pixel size of 64 nm within a field of view of 65 μm for the presented measurement. The sample was scanned using the Zernike phase contrast mode, acquiring 701 projections in 180° rotation with an acquisition time of 140 s per projection. The 3D data reconstruction was performed with Zeiss' proprietary software 'Scout and Scan Reconstructor', based on a filtered back projection algorithm. For the 2D and 3D visualization, we employed the software Dragonfly.[20] A median filter was used for the data treatment, and the built-in deep learning tools were used to quickly and accurately segment the images.

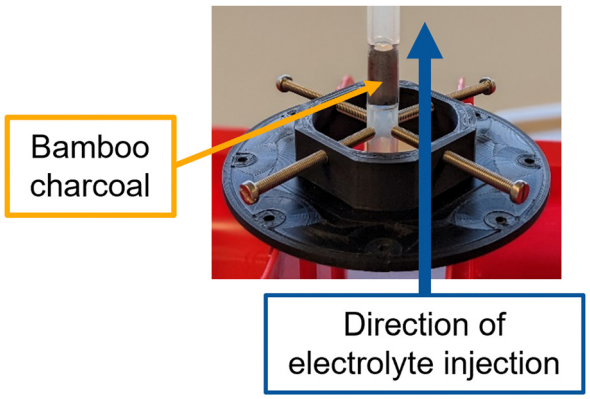

Fig. 2 Measurement setup for injection experiments with a synchrotron X-ray beam.

For the synchrotron-based *in situ* imaging measurements a dedicated experimental set-up was developed, detailed in Fig. 2. In particular, the bamboo charcoal tube was cut into a roughly 3 cm long piece and the large hole in the tube's center was filled with silicone construction foam to ensure that the electrolyte invades the channels of the bamboo charcoal. After hardening the foam, the filled bamboo charcoal piece was put into a heat shrink tubing with two tubing pieces placed on the top and the bottom. A small gap between the bamboo charcoal tube and the tubing pieces ensures that the tubing does not block the channel structure of the bamboo. The heat shrink tubing was shrunk with a heat gun and subsequently put in an oven to ensure it was fully contracted and no electrolyte could pass between the heat shrink tubing and the bamboo charcoal tube.

A vanadium electrolyte with 0.1 M V(IV) in 2 M H_2SO_4 was used to study the injection and flow through behavior of the electrolyte. The electrolyte was injected with a flow velocity of 1 mL min^{-1} into the bamboo charcoal tube using a syringe pump (LA-100, LANDGRAF LABORSYSTEME HLL).

All synchrotron measurements were performed with a white beam delivered from a superconducting wiggler located at the IMAGE beamline of the KIT Light Source. Filtered with 6 mm pyrolytic graphite, the spectrum results in a photon flux density of 2.7 × 10^{13} ph s^{-1} mm^{-2} at the sample position and a wide energy distribution centered at 14.5 keV. In order to exploit both the absorption and phase contrast, the wavefield transmitted through the sample was free space propagating 40 cm from the sample exit plane to the image plane before being detected by an X-ray detector. The detector was composed of a scintillator-based microscope (Elya solution) with a 200 μm LuAG:Ce scintillator (Crytur) and a Nikkor eyepiece (NIKON 85 mm f/1 : 1.4D, f-number = 4) providing a 3× magnification, and coupled with a Phantom v2640 fast camera (AMETEK, physical pixel size 13.5 μm × 13.5 μm), allowing to realize a field of view (FOV) of 9.2 mm × 8.8 mm (H × V) mm with a sufficiently small effective pixel size of 4.5 μm. The spatial resolution limit of the detection system is 9 μm.

To follow the electrolyte invasion in the bamboo charcoal, we recorded a cine-radiographic sequence at a frame rate of 500 frames per second (fps). Shortly before the electrolyte injection

was triggered, the camera recording was started to ensure that the onset of the injection process was fully captured. Tomography scans of the dry and imbibed BC tubes were conducted before and after the electrolyte injection by acquiring 3000 projections at 100 fps. For both the radiography and tomography experiments also dark field and flat field images were recorded to subtract the thermal noise from each projection and correct the different sensitivity of the pixels to the impinging light. Both absorption contrast and edge enhancement by phase contrast were utilized to distinguish the low absorbing electrolyte from the BC.[22] The 3D tomographic reconstruction was performed by using the tofu processing toolkit.[23]

Electrochemical characterization

CV and EIS investigated the electrochemical performance of undoped and N-doped BC. The measurements were performed in a three-electrode setup with an in-house developed flow cell[24] and an SP-300 potentiostat (BioLogic Science Instruments). The BC electrodes were prepared as rectangular pieces (1.0 cm × 1.0 cm) from the BC tubes using a jigsaw and sandpaper. The BC pieces were placed in the working electrode (WE) of the flow cell's channel and contacted by a gold foil (0.25 mm, 99.9975+%, Alfa Aesar) and a gold wire (∅ 0.5 mm, 99.9975+%, Alfa Aesar). In all experiments, an in-house developed hydrogen reference electrode (RHE) was used as the reference electrode (RE), and a stack of three thermally activated carbon papers (2.5 cm × 2.5 cm) served as the counter electrode (CE). The carbon paper stack was contacted with a titanium foil (1.0 mm, 99.2%, Alfa Aesar) and a gold wire. The CVs were conducted at room temperature with a scan rate of 2 mV s^{-1} while no flow was applied. Potential limits were chosen so the peaks were evident during the positive-going and negative-going scans.

EIS characterized the wettability and processes in the positive half-cell in the same setup as the CVs. The EIS measurements were performed at room temperature at a flow rate of 4 mL min^{-1} in a frequency range from 100 kHz to 3.5 mHz. The potentiostatic mode was used with a single sinusoidal excitation of 5 mV as the perturbation and an applied potential of 1.05 V *vs.* RHE. During the measurement, the electrolyte was pumped from the electrolyte reservoir through the flow cell and back to the reservoir by a peristaltic pump (Masterflex L/S, Cole-Parmer). Since the conditions at the electrodes should remain constant to gain meaningful impedance data, the electrolyte was continuously pumped to ensure a steady state.

The data were further analyzed using a MATLAB-based tool called 'DRTtools'[25] based on the Tikhonov regularization. The spectra fitting is based on a Gaussian function for the discretization and includes the inductive data. A regularization parameter of E-9 was used.

DVS

DVS measurements were performed with a Q5000 Sorption Analyzer (TA Instruments) to study the wettability of the BC. Two different measurements were conducted for each sample.

For the first measurement, the sample is heated up to 60 °C for 300 min at the beginning and end to remove water residues. Sorption and desorption isotherms under nitrogen gas flow at 25 °C are measured between 0% and 90% relative humidity (RH). The RH was changed stepwise by 5% and kept for 90 min at each RH (except for 120 min at 80% and 85% RH and 180 min at 90% RH).

A second measurement protocol was applied to reach a mass equilibrium after each sorption/desorption step. Here, the sample was again heated up to 60 °C at the beginning and the end of the measurement for 200 min. The measurement itself was conducted at 25 °C. After an initial step at 0% RH for 200 min, 20%, 40%, and 60% RH was kept for 600 min during sorption and desorption. Before heating up to 60 °C at the end of the measurement, 0% RH was kept for 300 min.

Results and discussion

This section highlights the feasibility of using BC as a renewable electrode material for VRFBs. SEM and X-ray imaging results are presented, which were applied to the ''static'' study of the morphology of dry BC as well as to the ''dynamic'' characterization of the *in situ* electrolyte flow in the BC electrode. Next, DVS experiments are presented to investigate the material's wettability in more detail. Finally, the electrochemical performance of BC was assessed by EIS and CV.

Structure

The characteristic structure of the investigated bamboo is displayed in Fig. 3a. The structure remains intact during the carbonization process. The top view SEM image (Fig. 3b) evidences the presence of large holes, which belong to channels leading through the whole BC tube. These channels have diameter ranging from around 20 μm to 100 μm and are surrounded by relatively dense parenchyma cells, which comprise most of the material. Cylindrical-shaped cells are also visible in the side view as rounded rectangular structures. The zoom-in on one of those cells reveals small holes, which interconnect the cells and might offer additional electrolyte pathways. Zhang *et al.*[4] investigated several BC samples using SEM with very high resolution. They observed the connecting holes in all samples. The pore sizes and volumes were studied by mercury injection. The results can be found here.[7]

Using SEM, it is only possible to analyze the sample surface. Therefore, we employed X-ray tomography to visualize the internal 3D structure of BC and verify whether it is suitable for electrolyte transport. The μ-CT volume rendering results in Fig. 3c and the video in the ESI† (Video S1) display the 3D structure of an undoped BC tube piece. Several large straight channels are visible, spreading through the whole material. The straight channels have various diameters ranging from around 20 μm to 100 μm, which is in agreement with the SEM study. Thus, the manufactured BC electrode is suitable for the electrolyte uptake during the electrochemical process (see Fig. 3c). The μ-CT image supports the previous observations from the

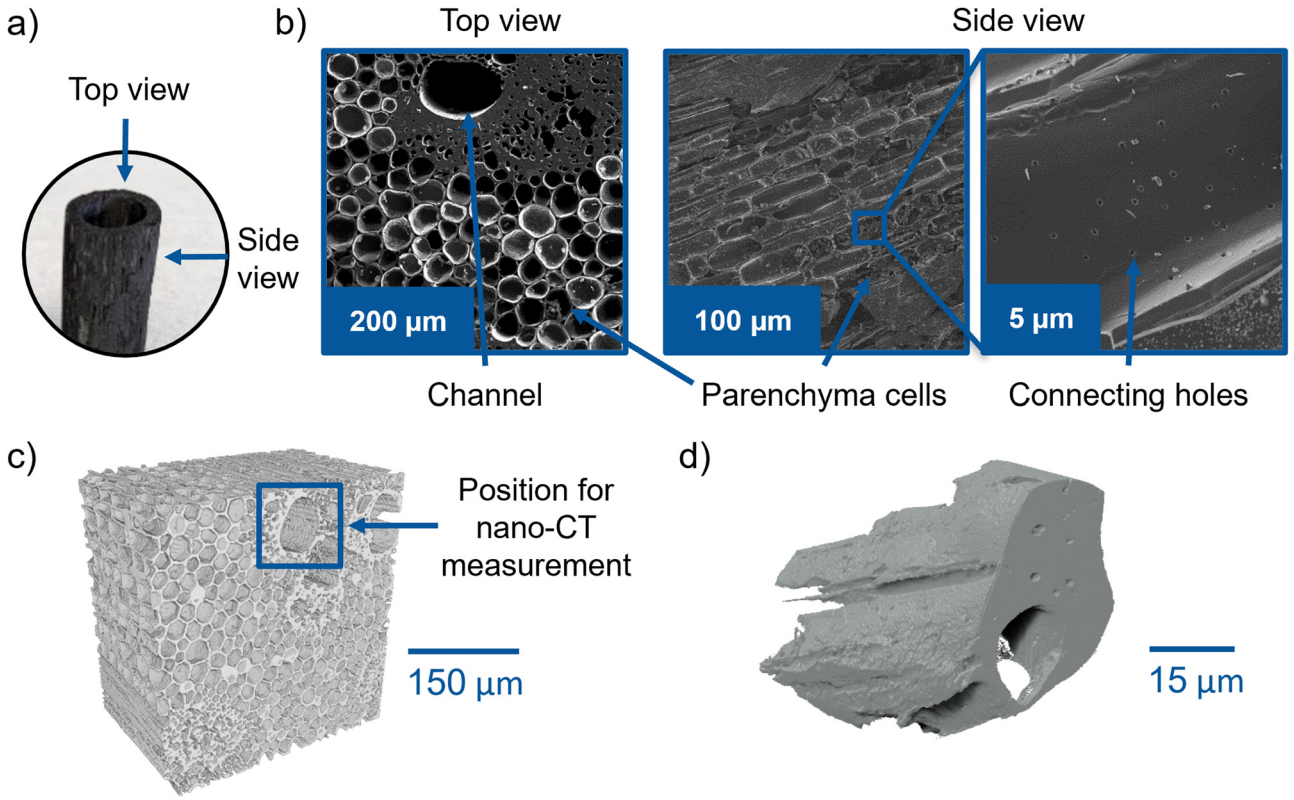

Fig. 3 Structure of undoped BC visualized by multiple imaging methods: (a) photograph of a BC tube (also showing the view directions); (b) SEM images conducted from different views and with different magnifications. (c) µ-CT volume rendering on a micrometer scale (FOV = 2 mm, pixel size = 2 µm) (d) nano-CT volume rendering on sub-micron scale (FOV = 64 µm, pixel size = 64 nm).

SEM images that the channels are surrounded by small, dense-packed cells, a very dense part of material directly around the channel, and larger parenchyma cells. The reconstructed slices of the channel structure through the whole BC volume are documented in Video S1 (ESI†).

The SEM image in Fig. 3b (zoom-in, side view) points out the presence of small connecting holes between the individual parenchyma cells. Since the resolution of the µ-CT is insufficient to study this feature, a small piece of bamboo was cut with a scalpel and investigated by nano-CT, which offers a higher spatial resolution. The nano-CT 3D volume rendering in Fig. 3d shows the presence of channels in the BC that extend straight through the scanned piece and a surrounding dense part with small holes – a feature observed in the upper right of the top view SEM image in Fig. 3b. Unfortunately, the nano-CT resolution is not high enough to study also the small connecting holes. However, in general, the visualized 3D structure of BC seems to be very promising for electrolyte transport owing to the differently sized channels and holes in the material. In the following section, the wettability of the material is investigated *via* synchrotron X-ray imaging and DVS to probe the structure for its ability to accommodate the electrolyte flow.

Wettability

This section investigates the wettability of BC. First, the synchrotron X-ray imaging techniques were employed to visualize the electrolyte injection behavior into a piece of BC, followed by a DVS study of differently treated materials. For the synchrotron experiments, the inner hollow part of an undoped BC tube was filled with a silicone construction foam to force the electrolyte through the bamboo channels. In the grayscale slices in Fig. 4a, the silicon construction foam corresponds to the bright circumference section, while the reconstructed darker fraction of the circular sector stands for the BC electrode. As described in the Experimental section, the vanadium electrolyte was injected from the bottom to the top of the BC piece, following the direction of the large channels. X-ray tomograms were recorded before and after the electrolyte injection in the BC to investigate the dry and imbibed channels and to prove whether the channel structure enables the electrolyte flow. The corresponding results are displayed in Fig. 4, which presents the top view (a), the side view (b), and the 3D renderings and segmentation of the filled channels (c) in the tomograms conducted before (dry, left image) and after (wet, center image) the electrolyte injection, respectively. Compared to the tomogram of the dry sample, the tomogram of the wetted BC reveals some brighter regions, thus indicating the presence of the electrolyte. The image on the right side displays the difference between the wet and dry image states, depicting the electrolyte in purple to bright yellow color scale, with yellow corresponding to larger differences. In conclusion, both, the top and the side views, confirm that the electrolyte was injected in the BC channels.

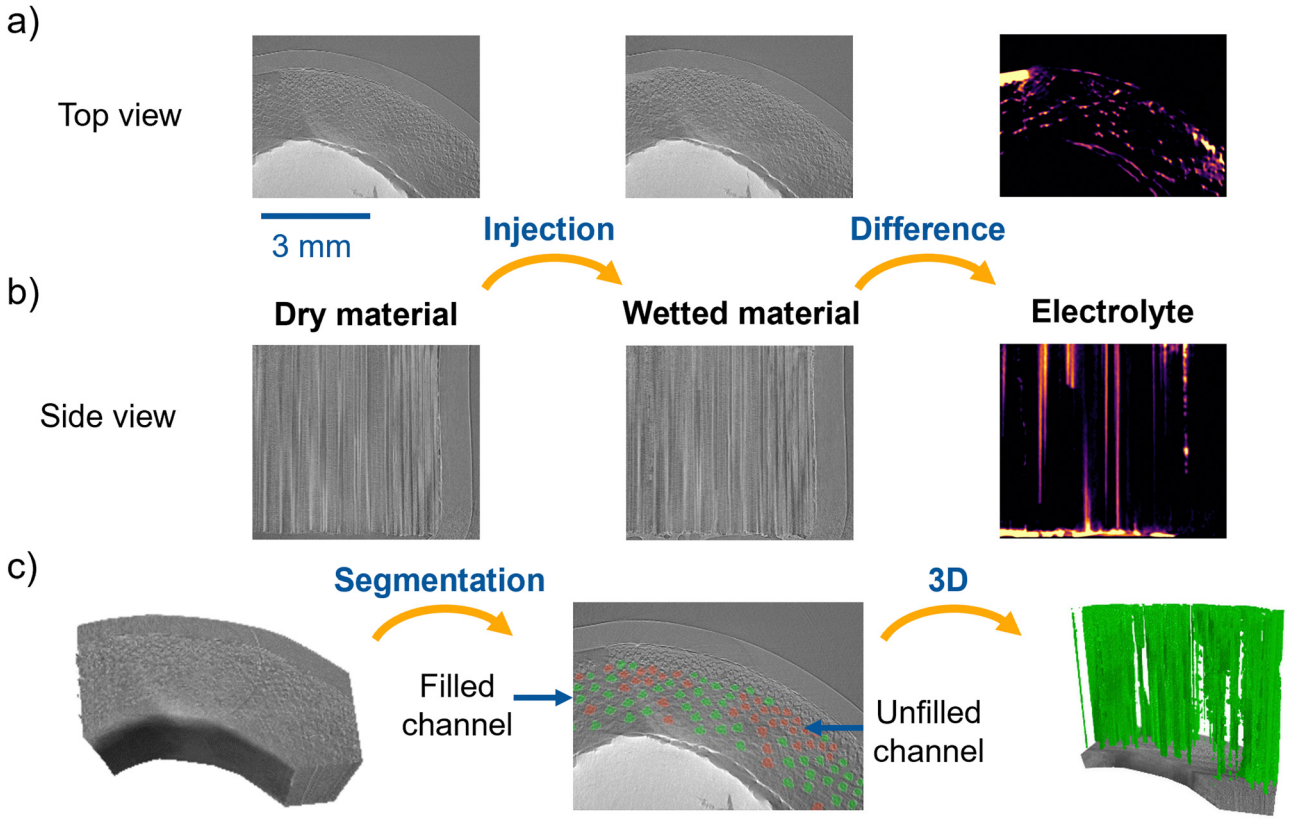

Fig. 4 BC channel morphology and electrolyte filling: (a) 2D top and (b) side view of synchrotron X-ray tomograms conducted before (dry, left) and after (wet, center) electrolyte injection into a BC piece and corresponding images showing the difference between both tomograms (right); (c) 3D display of the respective tomogram (left) and the segmentation process (center; green: filled channel, red: unfilled channel) to achieve a 3D rendering of filled channels (right).

The left and middle parts of Fig. 4c present the tomogram and the segmentation process, displaying the empty (depicted in red) and the filled (depicted in green) channels. Meanwhile, the right part presents the segmented filled channels. To quantitatively estimate the fraction of filled/unfilled channels, we have used the difference image between the wetted and dry material on a single 2D cut along the channel direction (see Fig. 4c, center) to guide the classification of each channel. The filled and unfilled channels correspond to 58.4% and 41.6%, respectively. This proves that injecting the electrolyte in the channel structure is possible and thus, the material's structure is meaningful for a flow battery.

To monitor *in situ* the electrolyte injection at a higher frame rate, we recorded a cine-radiographic sequence at 500 fps. Here, the whole bamboo structure is superimposed into a single image, making it difficult to discriminate between empty or filled channels. To overcome this, we performed an image subtraction of a reference image representing the bamboo structure at a given starting point to all the subsequent radiographs measured during the electrolyte flow. More precisely, the reference image was obtained by averaging 10 radiographic images recorded before the electrolyte started to invade the channels of the region being analyzed. We further applied a Gaussian blur filter to the difference images to minimize the image noise. The difference images resulting from the applied post-processing allowed us to visualize the filling of the channels during the electrolyte injection.

Representative difference images are displayed in Fig. 5, showing the channel filling process during injecting the electrolyte in the undoped BC. The selected radiographs represent a short sequence of the injection process. The bright and the dark image values correspond to the electrolyte and the empty BC, respectively. The direction of the electrolyte flow is bottom-up. The first image on the left side of Fig. 5 is recorded at a time T_1 and shows only a small amount of electrolyte, which started to enter the channels within the chosen region of interest. In the following difference images, sparsely selected from the measured sequence, the electrolyte progressively invades the channels from the bottom part and gradually fills the injected channels up to the top. Here, it takes about 0.4 s for the electrolyte to fill up the channels in the shown region of interest. Thus, the filling process of the channels is relatively swift with an average speed of 10 mm s^{-1} with up to 15 mm s^{-1} in the observed region of interest. On the right side of the image at Δ0.2 s after T_1, the electrolyte also invaded the parenchyma cell structure (see the roundish, bright part on the middle of the right edge; highlighted with an orange circle). This region was close to the edge of the studied BC piece. The BC was placed in a shrinking tube to force the electrolyte into the BC, which does not have an entirely smooth structure and

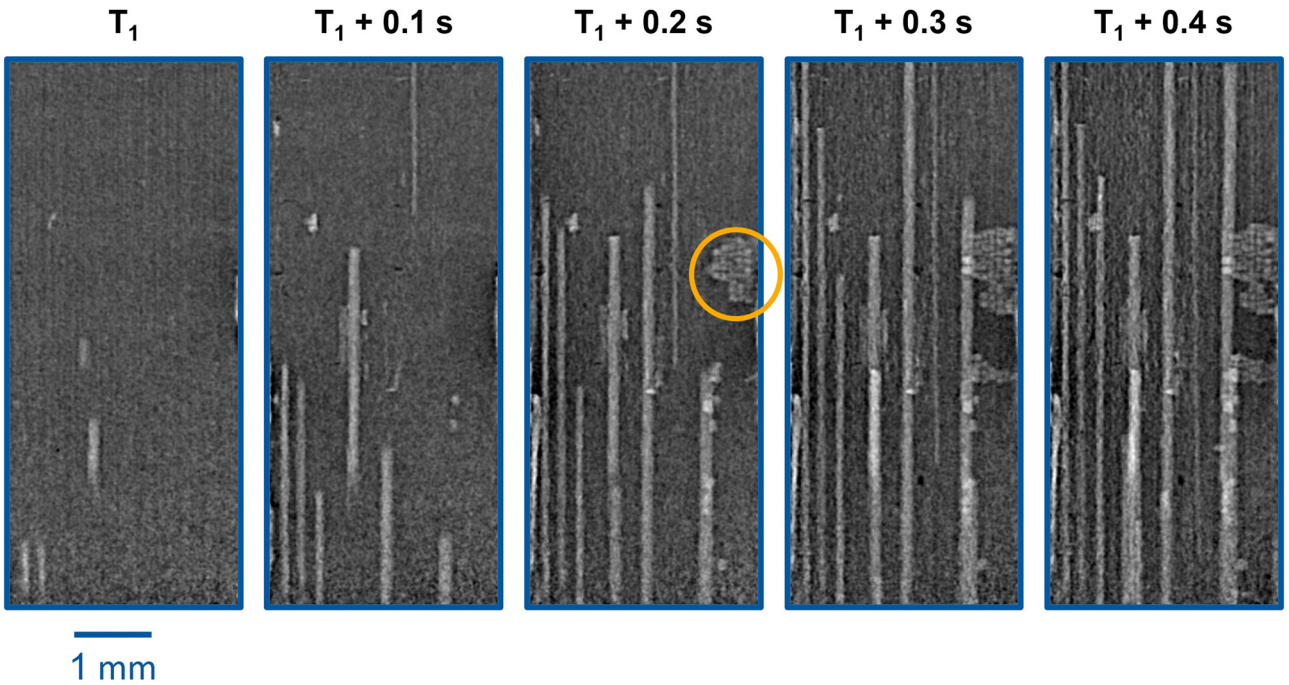

Fig. 5 Sequence of representative radiographs selected from synchrotron X-ray *in situ* 2D radiography experiment showing electrolyte injection in the BC tube.

surface. Due to that, some electrolytes passed between the BC and the shrinking tube and then invaded parts of the structure (see the right side of the images). The local invasion of the BC electrode edge may also explain the presence of a bright area in the top left side of the difference image in Fig. 4a, indicating a wet region larger than the typical BC channels.

In conclusion, synchrotron X-ray imaging enabled us to visualize the *in situ* electrolyte flow injection into the BC material's channel structure, demonstrating that BC has a suitable structure that benefits electrolyte transport. Given that synchrotron X-ray imaging cannot be employed in everyday experiments due to the limited beamtime available and the

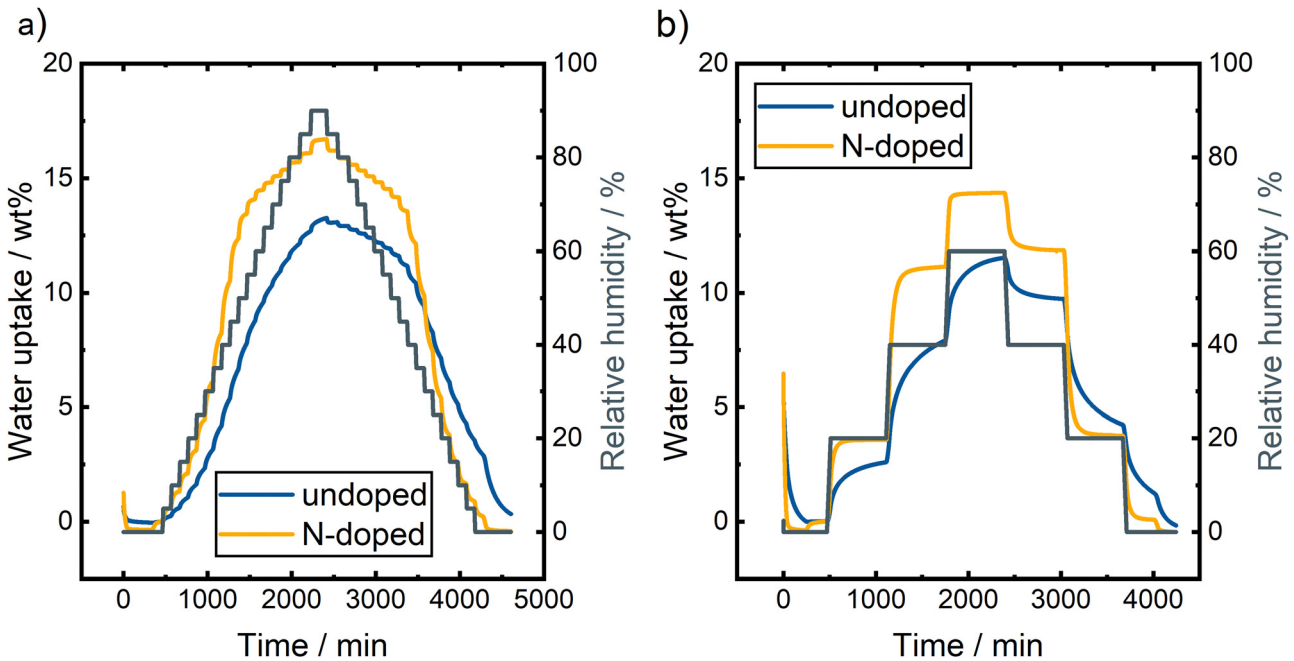

Fig. 6 DVS measurements of undoped and N-doped BC applying different measurement procedures with (a) 5% RH steps up to 90% RH and (b) 20% RH steps with longer duration up to 60% RH.

extensive preparation efforts, we introduce DVS measurements as an alternative method to quantify the BC wettability. However, this method can only provide information about the bulk wettability and not into the electrolyte imbibition, flow behavior, or local electrolyte distribution such as synchrotron X-ray imaging. DVS measures the weight change of a sample during the sorption and desorption of water vapor at defined RHs.

Here, we studied the sorption/desorption of water vapor for undoped and N-doped BC. Two different measurement protocols were used to study the samples in detail. During one procedure, the RH increases and decreases stepwise by 5% between 0% RH and 90% RH (Fig. 6a). The other measurement focuses on fewer RH steps with longer duration, increasing and decreasing the RH stepwise by 20% from 0% RH to 60% RH (Fig. 6b).

Generally, both samples take up more water at higher RH, with the N-doped sample adsorbing more water during both measurements and reaching equilibrium faster. Compared to commercial carbon felts, these samples show a significantly higher wettability and take up several times as much water as pristine or thermally activated carbon felts.[26,27]

Fig. 6a displays the DVS measurements of undoped and N-doped BC using the measurement protocol with 5% steps up to 90% RH. The undoped BC has a maximum weight change of 13.2 wt% at 90% RH. However, the given number does not fully reflect the maximum amount of adsorbed water since the sorption process for the undoped BC is relatively slow and does not reach an equilibrium at higher RH steps. At low RH (below 20%), the sorption equilibrium is reached for the undoped BC piece since less water is adsorbed. Contrarily, the sample takes up a significant amount of water, from 20% RH to 70% RH. Equilibrium is not reached here, and the weight change curve is still very steep even after a longer waiting period at the respective RH. Above 70% RH, no equilibrium is reached, and the adsorption is not finished before the desorption starts. During the desorption, an equilibrium is achieved above 50% RH since only a low amount of water is desorbing at high RHs. Monitoring the weight change below 50%, RH revealed significantly decreasing weight with decreasing RH; an equilibrium is not reached in this range again. We decided to forego sorption/desorption isotherms of the DVS data since the equilibrium is not reached at many RHs. However, basic information can also be gained from the time-resolved data. The strong hysteresis, caused by the differences in sorption and desorption behavior of water vapor, can already be noticed in Fig. 6a. Strong hysteresis is usually caused by strong hydrogen bond interactions between water molecules and pore blocking due to condensation within the porous structure.[28–30]

As mentioned previously, a second DVS experiment was performed with undoped BC (Fig. 6b). Here, only a few selected RH steps were investigated to gain more information about the duration of the sorption and desorption processes. In general, this measurement for undoped BC shows the same behavior. At a low RH of 20%, the equilibrium weight is almost reached, but at higher values of 40% RH and 60% RH, the weight changes even after an equilibration time of 10 h. A stable weight can be achieved at a higher RH during desorption. Nevertheless, the weight changes significantly at the end of the step at 20% RH. After heating the sample to 60 °C, the starting weight is reached, proving the full reversibility of the water sorption at the undoped BC.

The N-doped BC shows larger weight changes during the DVS measurements. During the procedure with several 5% RH steps, a maximum weight change of 16.7 wt% was observed at 90% RH compared to 13.2 wt% for the undoped sample (Fig. 6a). At low and high RH, the weight is stable at the end of the steps. However, no equilibrium is reached in the range of 25% RH to 60% RH, and the weight changes significantly even at the end of the step. Such strong weight changes can be attributed to the multilayer adsorption of water molecules. Again, we decided not to display the data as sorption/desorption isotherms since no stable weight is reached during some RH steps. However, the time-resolved plot demonstrates the high reversibility of the sorption/desorption process on N-doped BC. The starting weight was reached after the desorption steps, proofing the full reversibility of the water vapor sorption. Furthermore, the shape of the curve is symmetrical for the sorption and desorption processes. Thus, the hysteresis would be minimal, indicating a similar sample behavior during both processes.

The second measurement protocol with fewer steps was also used to investigate the N-doped BC. The result is displayed in Fig. 6b. A stable weight was reached during all measurements, indicating that the sorption and desorption processes at the sample's surface are faster than the undoped BC. A comparison of the weight change at different steps also demonstrates the high reversibility of the processes. At 0% RH, the same weight was reached after the sorption/desorption process, and at 20% RH, only a neglectable weight change was monitored with 3.6 wt% and 3.7 wt% for the adsorption and desorption, respectively. A slight weight difference of 0.7 wt% was observed at 40% RH (11.1 wt% *vs.* 11.8 wt%), which shows that the reversibility is worse when more water vapor is adsorbed initially.

In summary, both samples show high wettability and reversibly adsorb high amounts of water vapor. Combined with the results from the synchrotron X-ray imaging experiments, the DVS measurements prove that both BC samples exhibit a promising wetting behavior and an intrinsic structure suitable for electrolyte transport.

Electrochemical performance

In addition to the synchrotron X-ray imaging and the DVS experiments, EIS measurements were performed to assess the wettability using another approach. To differentiate and gain more insights into the processes occurring in the electrode material, we use EIS coupled with DRT analysis. DRT analysis is a well-suited tool to assign peaks in a DRT spectrum to physical processes and to study the effects of different conditions. Our group established this analysis tool for VRFB research, identifying processes in three different frequency ranges in various DRT spectra. The high-frequency (HF) range provides

information about the electrochemical reaction, whereas the mid-frequency (MF) range helps to investigate the transport processes in the porous structure of the electrode. We can determine additional information about ion transport based on the impedance in the low-frequency (LF) range.[24] DRT analysis is also used to link the material's wettability to its surface morphology.[26,27]

We performed EIS measurements of the undoped and N-doped BC at a potential of 1.05 V *vs.* RHE, which triggers the V(IV) to V(V) reaction. The BC was cut into rectangular pieces of 1 cm^2 and inserted into the flow cell. As observed in the previous section, the piece was placed in the flow direction to ensure a flow through the channel structure. The setup is described in detail in the Experimental section and a previous study by Schilling *et al.*[24] It mimics the conditions in a commercial VRFB. It enables experiments under steady-state conditions required for reliable EIS data.

The Nyquist plots of both samples' EIS measurements are presented in Fig. 7a. The spectra consist of several superimposed semicircles and a straight line at lower frequencies. However, it is difficult to determine the number of underlying semicircles by eye. DRT analysis separates the individual contributions of the processes to the overall impedance by determining the number of RC elements that best reflect the data.[31,32] The DRT spectra of both samples are displayed in Fig. 7b. An overall impedance of 168 Ω was determined for the undoped BC and 96 Ω for the N-doped BC. The spectra are divided into three different frequency ranges based on previous studies.[24,26,27,33,34] Above 100 Hz, one peak was observed for both samples, associated with the electrochemical reaction. The peak position provides information about the rate-determining step of the reaction. The peak of the N-doped BC is shifted to higher frequencies than the peak of the undoped BC. Thus, the V(IV)/V(V) reaction proceeds faster in N-doped BC. Furthermore, the area under the peak corresponds to the peak's impedance assigned to a specific process. Here, the HF impedance with the undoped BC electrode is three times larger than with the N-doped BC electrode. Thus, the N-doping is beneficial for the reaction kinetics and helps to catalyze the reaction. Nevertheless, the peaks for both materials are rather broad, indicating that many sites with slightly different catalytic activity exist. Since BC is derived from natural bamboo, inhomogeneities in the sample can be expected. The peaks in the MF range (2 mHz–100 Hz) and LF range (below 2 mHz) depend on the transport properties of the sample. The LF peak is caused by the ion transport, and contributes the most to the overall impedance with 89% for both the undoped BC and the N-doped BC. This result also follows the DVS results which revealed a higher wettability for the N-doped BC. In the MF range, several peaks are observed due to the complex BC structure. However, some peaks are at the same position in the DRT spectra for both samples (*e.g.*, 0.01 Hz and 0.05 Hz) since the general structure of undoped and N-doped BC is identical.

Nevertheless, the materials must be optimized for the electrolyte flow. Larger channels could achieve lower transport-related impedances, either breaking up the existing structure or using a different kind of raw bamboo material.

The electrochemical performance of the materials was further evaluated by CV in the same flow cell setup. To obtain more information about the materials' catalytic activity for VRFB application, we investigated the V(IV)/V(V) reaction of the positive VRFB half-cell in more detail. The CVs are displayed in Fig. 8. The potential range was adapted to each material to cover all relevant parts of both scan directions.

In general, the CVs of both materials differ significantly. The undoped BC shows the typical duck shape for a reversible reaction described in the literature.[35] The peak-to-peak separation ΔE is 91 mV, proofing the high reversibility of the redox reaction and fast reaction kinetics. A charge ratio $C_{negative}/C_{positive}$ of 0.87 was determined, indicating good reversibility with a slightly higher charge transfer in the positive-going scan.

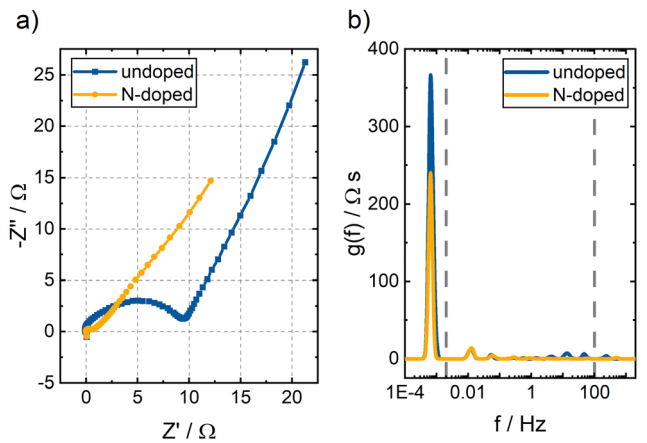

Fig. 7 (a) Nyquist plots and (b) DRT spectra of undoped and N-doped BC. A V(IV) electrolyte and a flow rate of 15 mL min^{-1} were used. A potential of 1.05 V *vs.* RHE was applied.

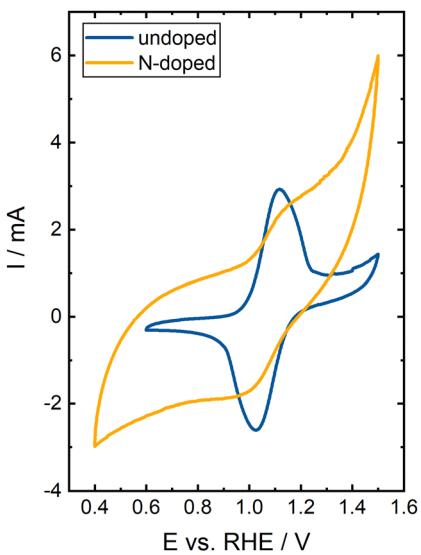

Fig. 8 CV of undoped and N-doped BC at a scan rate of 2 mV s^{-1} in V(IV) electrolyte.

At high positive electrode potentials, carbon materials are degraded due to carbon corrosion (CO_2 formation), a major issue for the VRFB performance.[36,37] Most likely, the deviation of the charge ratio from the ideal value of 1.00 is caused by this irreversible side reaction. Additionally, the microscopic and macroscopic structure of BC can influence the peak separation since it differs from the ideal, flat electrode.

The CV of the N-doped BC was not analyzed in detail since the key characteristics, such as charge ratio, maximum currents, or peak-to-peak separation, could not be identified. The catalytic activity towards the V(IV)/V(V) reaction significantly decreases since only a shoulder can be observed during the positive-going and negative-going scan for both vanadium redox reactions. Strong carbon corrosion occurs at higher potentials, significantly decreasing the overall efficiency. Some of the introduced active sites benefit the vanadium reaction since the HF peak in the DRT spectra is shifted to higher frequencies. Additionally, the HF impedance is decreased. Nevertheless, the harsh reaction conditions during N-doping introduce many active polar sites. However, these sites are not active towards the desired vanadium reaction. Thus, N-doping enhances the wettability but decreases the performance due to more carbon corrosion side reactions.

Conclusions

In this study, we investigated BC as a potential electrode material for VRFBs for the first time. Several techniques were used for investigating the structure, the wettability and wetting behavior, and the electrochemical performance of the material. The aim is to identify a material with suitable wettability and catalytic activity towards the vanadium species.

Bamboo tubes were used as raw material to prepare undoped and N-doped BC samples. The structure of BC was investigated with imaging techniques (SEM, μ-CT, and nano-CT) confirming that BC has a promising channel structure and interconnecting pores, which can be used for electrolyte transport. Synchrotron X-ray imaging allowed us to visualize *in situ* the electrolyte injection as well as the electrolyte distribution in the undoped material, proofing that the channel structure is indeed used for electrolyte transport. Thus, the wetting behavior of this material is very promising. DVS measurements demonstrated a very high water vapor sorption by both materials with a slightly higher wettability of the N-doped BC. Finally, we studied the electrochemical performance of the differently-doped BC samples. The undoped BC sample performed excellently during the CV study, whereas the N-doped BC demonstrated less catalytic activity and a higher tendency to the carbon corrosion side reaction. The EIS measurements combined with DRT analysis revealed that 89% of the overall impedance is caused by the ion transport in both samples. However, the N-doped BC has a significantly lower overall impedance than the undoped BC.

In conclusion, the presented study demonstrates that BC might be a promising electrode material for VRFBs due to its high wettability, natural flow channel structure, and electrochemical activity. Furthermore, bamboo is a sustainable and renewable resource that grows easily and quickly. The high impedance values for the transport-related processes show that the flow properties must be further optimized. Therefore, another kind of raw bamboo with larger channels might be suitable, or the existing structure must be modified, *e.g.*, by breaking up the channel structure. Suitable BC electrodes for full-cell tests should be prepared as the next step. Conducting full-cell tests is necessary to prove that BC is another potential candidate for VRFB electrodes for large-scale energy storage.

Author contributions

Monja Schilling: conceptualization, investigation, data curation, data analysis (all), methodology, writing – first draft; Rafaela Debastiani: data curation (nano-CT), writing – review and editing; Alexey Ershov: data curation, data analysis (nano-CT, X-ray imaging), writing – review and editing; Kangjun Duan: data analysis (μ-CT), writing – review and editing; Kerstin Köble: data curation, data analysis (X-ray imaging), writing – review and editing, Simon Scherer: data curation (CV, EIS, SEM), writing – review and editing; Linghan Lan: material preparation, writing – review and editing; Alexander Rampf: data curation (X-ray imaging), writing – review and editing; Tomáš Faragó: data curation, data analysis (X-ray imaging), writing – review and editing, Marcus Zuber: data curation, data analysis (X-ray imaging), writing – review and editing; Angelica Cecilia: data curation, data analysis (X-ray imaging), writing – review and editing; Shaojun Liu: material preparation; Cheng Liu: material preparation, writing – review and editing; Tilo Baumbach: supervision, funding acquisition, writing – review and editing; Jun Li: supervision, funding acquisition, writing – review and editing; Pang-Chieh Sui: supervision, funding acquisition, writing – review and editing; Roswitha Zeis: conceptualization, supervision, funding acquisition, writing – review and editing.

Conflicts of interest

There are no conflicts to declare.

Acknowledgements

M. S. gratefully acknowledges financial support through a Kekulé PhD fellowship by the Fonds der Chemischen Industrie (FCI) and the 'Financial support programs for female researchers' by the Office for Gender Equality Ulm University. We especially thank SGL Carbon for supplying the SIGRACET® carbon paper. This work was partly carried out with the support of the Karlsruhe Nano Micro Facility (KNMF, **https://www.knmf.kit.edu**), a Helmholtz Research Infrastructure at Karlsruhe Institute of Technology (KIT, **https://www.kit.edu**). The Xradia 810 Ultra (nano-CT) core facility was supported (in part) by the 3DMM2O – Cluster of Excellence (EXC-2082/

1390761711). R. D. acknowledges the support of the Cluster of Excellence 3DMM2O (EXC_2082/1-390761711), funded by the German Research Council (DFG). K. D. acknowledges financial support from the China Scholarship Council under grant number 202106950013. This work contributes to the research performed at CELEST (Center for Electrochemical Energy Storage Ulm-Karlsruhe). R. Z., J. L. and P. C. S. acknowledge the financial support from the Sino-German Mobility Programme (M-0070). C. L. acknowledges the support of the Fundamental Research Funds for the Central Universities of China (2021-JL-003).

References

1 SGL CARBON GmbH, SIGRACELL battery felts – Datasheet (**https://www.sigracell.com**), 2019.
2 R. Schweiss, C. Meiser, T. Damjanovic, I. Galbati and N. Haak, SIGRACET Gas Diffusion Layers for PEM Fuel Cells, Electrolyzers and Batteries. White Paper, **https://www.fuelcellstore.com/spec-sheets/sigracet-gdl-white-paper-new-generation.pdf**, (accessed 29 March 2022).
3 K. J. Kim, M.-S. Park, Y.-J. Kim, J. H. Kim, S. X. Dou and M. Skyllas-Kazacos, A technology review of electrodes and reaction mechanisms in vanadium redox flow batteries, *J. Mater. Chem. A*, 2015, **3**, 16913–16933.
4 Y. Zhang, W. Yang, Q. Fu, J. Li, X. Zhu and Q. Liao, Performance optimization of microbial fuel cells using carbonaceous monolithic air-cathodes, *Int. J. Hydrogen Energy*, 2019, **44**, 3425–3431.
5 W. Yang, J. Li, L. Zhang, X. Zhu and Q. Liao, A monolithic air cathode derived from bamboo for microbial fuel cells, *RSC Adv.*, 2017, **7**, 28469–28475.
6 X. Liu, M. Chen, Q. Xu, K. Gao, C. Dang, P. Li, Q. Luo, H. Zheng, C. Song, Y. Tian, H. Yao, Y. Jin, Y. Xuan and Y. Ding, Bamboo derived SiC ceramics-phase change composites for efficient, rapid, and compact solar thermal energy storage, *Sol. Energy Mater. Sol. Cells*, 2022, **240**, 111726.
7 L. Lan, W. Yang, J. Li, L. Zhang, Q. Fu and Q. Liao, Membrane-less Direct Formate Fuel Cell Using an Fe-N-Doped Bamboo Internode as the Binder-Free and Monolithic Air-Breathing Cathode, *ACS Appl. Mater. Interfaces*, 2020, **12**, 27095–27103.
8 C.-S. Yang, Y. S. Jang and H. K. Jeong, Bamboo-based activated carbon for supercapacitor applications, *Curr. Appl. Phys.*, 2014, **14**, 1616–1620.
9 Y.-C. Chang, Y.-C. Shih, J.-Y. Chen, G.-Y. Lin, N.-Y. Hsu, Y.-S. Chou and C.-H. Wang, High efficiency of bamboo-like carbon nanotubes on functionalized graphite felt as electrode in vanadium redox flow battery, *RSC Adv.*, 2016, **6**, 102068–102075.
10 R. Madhu, F. V. Kusmartsev, K. Kim and H.-J. Ahn, Flexible and free-standing electrode for high-performance vanadium redox flow battery: Bamboo-like carbon fiber skeleton from textile fabric, *Electrochim. Acta*, 2023, **439**, 141619.
11 Y. Sun, R. B. Sills, X. Hu, Z. W. Seh, X. Xiao, H. Xu, W. Luo, H. Jin, Y. Xin, T. Li, Z. Zhang, J. Zhou, W. Cai, Y. Huang and Y. Cui, A Bamboo-Inspired Nanostructure Design for Flexible, Foldable, and Twistable Energy Storage Devices, *Nano Lett.*, 2015, **15**, 3899–3906.
12 J. Mei, X. Peng, Q. Zhang, X. Zhang, T. Liao, V. Mitic and Z. Sun, Bamboo-Membrane Inspired Multilevel Ultrafast Interlayer Ion Transport for Superior Volumetric Energy Storage, *Adv. Funct. Materials*, 2021, **31**, 2100299.
13 W. Yang, J. Li, D. Ye, X. Zhu and Q. Liao, Bamboo charcoal as a cost-effective catalyst for an air-cathode of microbial fuel cells, *Electrochim. Acta*, 2017, **224**, 585–592.
14 J. Scurlock, D. C. Dayton and B. Hames, Bamboo: an overlooked biomass resource?, *Biomass Bioenergy*, 2000, **19**, 229–244.
15 L. Zou, H. Jin, W.-Y. Lu and X. Li, Nanoscale structural and mechanical characterization of the cell wall of bamboo fibers, *Mater. Sci. Eng., C*, 2009, **29**, 1375–1379.
16 L. Osorio, E. Trujillo, F. Lens, J. Ivens, I. Verpoest and A. W. van Vuure, In-depth study of the microstructure of bamboo fibres and their relation to the mechanical properties, *J. Reinf. Plast. Compos.*, 2018, **37**, 1099–1113.
17 F. L. Palombini, E. L. Lautert, J. E. D. A. Mariath and B. F. de Oliveira, Combining numerical models and discretizing methods in the analysis of bamboo parenchyma using finite element analysis based on X-ray microtomography, *Wood Sci. Technol.*, 2020, **54**, 161–186.
18 F. L. Palombini, W. Kindlein, B. F. de Oliveira and J. E. de Araujo Mariath, Bionics and design: 3D microstructural characterization and numerical analysis of bamboo based on X-ray microtomography, *Mater. Charact.*, 2016, **120**, 357–368.
19 M. K. Habibi, A. T. Samaei, B. Gheshlaghi, J. Lu and Y. Lu, Asymmetric flexural behavior from bamboo's functionally graded hierarchical structure: underlying mechanisms, *Acta Biomater.*, 2015, **16**, 178–186.
20 Object Research Systems (ORS) Inc., Dragonfly: 3D Visualization and Analysis Solutions for Scientific and Industrial Data, 2022.
21 K. Xia, Z. Dong, Q. Sun, R. Debastiani, S. Liu, Q. Jin, Y. Li, U. W. Paetzold, P. Gumbsch, U. Lemmer, Y. M. Eggeler, P. A. Levkin and G. Hernandez-Sosa, Electrical Conductivity and Photodetection in 3D-Printed Nanoporous Structures *via* Solution-Processed Functional Materials, *Adv. Mater. Technol.*, 2023, DOI: **10.1002/admt.202300408**.
22 D. Paganin, S. C. Mayo, T. E. Gureyev, P. R. Miller and S. W. Wilkins, Simultaneous phase and amplitude extraction from a single defocused image of a homogeneous object, *J. Microsc.*, 2002, **206**, 33–40.
23 T. Faragó, S. Gasilov, I. Emslie, M. Zuber, L. Helfen, M. Vogelgesang and T. Baumbach, Tofu: a fast, versatile and user-friendly image processing toolkit for computed tomography, *J. Synchrotron Radiat.*, 2022, **29**, 916–927.
24 M. Schilling, M. Braig, K. Köble and R. Zeis, Investigating the V(iv)/V(v) electrode reaction in a vanadium redox flow battery – A distribution of relaxation times analysis, *Electrochim. Acta*, 2022, **430**, 141058.
25 T. H. Wan, M. Saccoccio, C. Chen and F. Ciucci, Influence of the Discretization Methods on the Distribution of

Relaxation Times Deconvolution: Implementing Radial Basis Functions with DRTtools, *Electrochim. Acta*, 2015, **184**, 483–499.

26 K. Köble, M. Jaugstetter, M. Schilling, M. Braig, T. Diemant, K. Tschulik and R. Zeis, Multimodal characterization of carbon electrodes' thermal activation for vanadium redox flow batteries, *J. Power Sources*, 2023, **569**, 233010.

27 M. Schilling, L. Eifert, K. Köble, M. Jaugstetter, N. Bevilacqua, K. F. Fahy, K. Tschulik, A. Bazylak and R. Zeis, Investigating the Influence of Treatments on Carbon Felts for Vanadium Redox Flow Batteries, *ChemSusChem*, 2023, **17**, e202301063.

28 J. Alcañiz-Monge, A. Linares-Solano and B. Rand, Water Adsorption on Activated Carbons: Study of Water Adsorption in Micro- and Mesopores, *J. Phys. Chem. B*, 2001, **105**, 7998–8006.

29 L. Liu, S. J. Tan, T. Horikawa, D. D. Do, D. Nicholson and J. Liu, Water adsorption on carbon - A review, *Adv. Colloid Interface Sci.*, 2017, **250**, 64–78.

30 M. Thommes, K. Kaneko, A. V. Neimark, J. P. Olivier, F. Rodriguez-Reinoso, J. Rouquerol and K. S. Sing, Physisorption of gases, with special reference to the evaluation of surface area and pore size distribution (IUPAC Technical Report), *Pure Appl. Chem.*, 2015, **87**, 1051–1069.

31 N. Bevilacqua, M. A. Schmid and R. Zeis, Understanding the role of the anode on the polarization losses in high-temperature polymer electrolyte membrane fuel cells using the distribution of relaxation times analysis, *J. Power Sources*, 2020, **471**, 228469.

32 M. A. Danzer, Generalized Distribution of Relaxation Times Analysis for the Characterization of Impedance Spectra, *Batteries*, 2019, **5**, 53.

33 K. Köble, M. Schilling, L. Eifert, N. Bevilacqua, K. F. Fahy, P. Atanassov, A. Bazylak and R. Zeis, Revealing the Multifaceted Impacts of Electrode Modifications for Vanadium Redox Flow Battery Electrodes, *ACS Appl. Mater. Interfaces*, 2023, **15**(40), 46775–46789.

34 M. Schilling and R. Zeis, Analyzing the Processes in the Negative Half-Cell of a Vanadium Redox Flow Battery – A Distribution of Relaxation Times Analysis, *Electrochim. Acta*, 2024, **477**, 143771.

35 N. Elgrishi, K. J. Rountree, B. D. McCarthy, E. S. Rountree, T. T. Eisenhart and J. L. Dempsey, A Practical Beginner's Guide to Cyclic Voltammetry, *J. Chem. Educ.*, 2018, **95**, 197–206.

36 L. Eifert, Z. Jusys, R. J. Behm and R. Zeis, Side reactions and stability of pre-treated carbon felt electrodes for vanadium redox flow batteries: A DEMS study, *Carbon*, 2020, **158**, 580–587.

37 L. Eifert, Z. Jusys, R. Banerjee, R. J. Behm and R. Zeis, Differential Electrochemical Mass Spectrometry of Carbon Felt Electrodes for Vanadium Redox Flow Batteries, *ACS Appl. Energy Mater.*, 2018, **1**, 6714–6718.